VIP *Very Important Paper*

Surface Science and Electrochemical Model Studies on the Interaction of Graphite and Li-Containing Ionic Liquids

Isabella Weber,[a, b, c] Jihyun Kim,[b] Florian Buchner,[b] Johannes Schnaidt,[a, b, c] and R. Jürgen Behm*[a, b]

The process of solid–electrolyte interphase (SEI) formation is systematically investigated along with its chemical composition on carbon electrodes in an ionic liquid-based, Li-containing electrolyte in a combined surface science and electrochemical model study using highly oriented pyrolytic graphite (HOPG) and binder-free graphite powder electrodes (Mage) as model systems. The chemical decomposition process is explored by deposition of Li on a pre-deposited multilayer film of 1-butyl-1-methylpyrrolidinium bis(trifluoromethylsulfonyl)-imide ([BMP][TFSI]) under ultrahigh vacuum conditions. Electrochemical SEI formation is induced by and monitored during potential cycling in [BMP][TFSI] + 0.1 M LiTFSI. The chemical composition of the resulting layers is characterized by X-ray photoelectron spectroscopy (XPS), both at the surface and in deeper layers, closer to the electrode | SEI interface, after partial removal of the film by Ar^+ ion sputtering. Clear differences between chemical and electrochemical SEI formation, and also between SEI formation on HOPG and Mage electrodes, are observed and discussed.

Introduction

Lithium-ion batteries (LIBs) are heavily used in portable communication devices and in the transportation sector owing to their low self-discharge and memory effect, high specific energy, and long cycle lives.[1,2] Typically, they consist of Li^+-hosting electrode materials[3–5] and blends of carbonate solvents mixed with Li^+-containing salts as the electrolyte.[6–8] Despite considerable progress, however, LIBs still suffer—at least in part—from the use of flammable and/or poisonous electrolytes. On one hand, certain ionic liquids (ILs) have been shown to exhibit very low vapor pressures and, consequently, low flammability, while at the same time possessing the high electrochemical stability window that is required for the use of high-voltage cathodes.[9–14] Drawbacks, on the other hand, are their high viscosity, low conductivity, and currently high costs. Nevertheless, they have been carefully studied for potential battery applications.[15–23]

The key factor for the stability of a LIB is the so-called solid–electrolyte interphase (SEI), which is formed by decomposition of the electrolyte during charge and discharge.[24–27] It passivates the anode surface towards further electrolyte decomposition and thus prevents electrolyte depletion, while at the same time protecting the electrode from corrosion. Despite numerous studies, a microscopic understanding of the SEI formation process is still lacking; mainly because of the complex composition of electrodes and electrolyte in realistic systems. Here, model studies using simplified components and often also simplified preparation conditions come into play, allowing better identification of the significant processes and interactions. The disadvantage of these model studies is, however, that they may be of limited relevance for realistic systems/conditions.

In view of this, we report herein the results of a combined electrochemical and surface science-type model study on the formation of such passivation layers on well-defined basal surfaces of highly oriented, pyrolytic graphite (HOPG) electrodes and on binder-free graphite powder model electrodes, where the latter are closer to realistic systems, upon interaction with the IL 1-butyl-1-methylpyrrolidinium bis(trifluoromethylsulfonyl) imide [BMP][TFSI] and Li^0/0.1 M LiTFSI. This approach allows us to stepwise bridge the gap between idealized model studies performed under ultrahigh vacuum (UHV) conditions, and more realistic electrode material/SEI formation conditions.

The passivation layers were prepared either by vacuum deposition of [BMP][TFSI] and Li^0 on HOPG in UHV, or by potentiodynamic cycling of graphite electrodes in [BMP][TFSI] + 0.1 M LiTFSI electrolyte. By comparing the composition of the adlay-

[a] I. Weber, Dr. J. Schnaidt, Prof. Dr. R. J. Behm
Helmholtz-Institute Ulm (HIU) Electrochemical Energy Storage
Helmholtzstraße 11, 89081 Ulm (Germany)
[b] I. Weber, Dr. J. Kim, Dr. F. Buchner, Dr. J. Schnaidt, Prof. Dr. R. J. Behm
Institute of Surface Chemistry and Catalysis, Ulm University
Albert-Einstein-Allee 47, 89081 Ulm (Germany)
E-mail: juergen.behm@uni-ulm.de
[c] I. Weber, Dr. J. Schnaidt
Karlsruhe Institute of Technology (KIT)
P.O. Box 3640, 76021 Karlsruhe (Germany)
Supporting information and the ORCID identification number(s) for the author(s) of this article can be found under: https://doi.org/10.1002/cssc.202000495.

er/passivation layer created by these processes, as characterized by ex situ X-ray photoelectron spectroscopy (XPS), we want to i) learn about the role of the electrochemical conditions on the formation and composition of the resulting layer and ii) elucidate the effect of the graphite structure on IL decomposition/SEI formation. The process of electrochemical SEI formation was monitored by cyclic voltammetry (CV). Furthermore, depth profiling of the SEI was performed by Ar^+ sputtering; as well as sputtering of pure LiTFSI and [BMP][TFSI] to verify the influence of the Ar^+ beam.

This work is part of a comprehensive effort to better understand the electrochemistry and decomposition behavior of ILs, specifically of [BMP][TFSI], and typical salts such as LiTFSI. Owing to its high decomposition temperature, very low vapor pressure, and a large stability window ranging from −2.5 to 3.0 V versus Ag/AgCl (about 0–5 V vs. Li/Li^+),[15] [BMP][TFSI] is a very promising candidate for LIBs. Special interest was placed on the interactions at the substrate | IL interface under UHV conditions by using several model substrates,[28] for example, single-crystalline metal surfaces,[29–32] oxide surfaces,[33–35] and highly oriented pyrolytic graphite.[36,37] The above studies, which were conducted in the absence of an applied potential and which focused on the structure formation and the decomposition of the ionic liquid, clearly demonstrated that the chemical interaction with the substrate surface and/or with the added lithium is sufficient to cause decomposition of the IL. Moreover, there is a large number of electrochemical model studies investigating the interaction of [BMP][TFSI] with a variety of different electrodes under electrochemical conditions. Examples include Li (Li-coated Cu),[38,39] Pt,[40–42] Au,[40,42] and glassy carbon[40] as well as HOPG[43] and graphite composite electrodes.[44] These studies revealed that the comparatively large stability window of [BMP][TFSI] is greatly influenced and diminished by the presence of traces of moisture and other contaminants.[41,42,45–47] Electrolyte degradation has been reported to progress through reductive $[TFSI]^-$ decomposition[23,38,39,43] and subsequent SEI formation/surface passivation.[43] In addition, the presence of 0.12 M of LiTFSI has been shown to enhance $[TFSI]^-$ decomposition on Pt in [EMIm][TFSI] ([EMIm]: 1-ethyl-3-methylimidazolium).[48] Furthermore, by employing in situ scanning tunneling microscopy (STM), Hu and co-workers observed that reductive cation decomposition takes place in the first cathodic scan when cycling a HOPG electrode in 0.5 M LiTFSI-containing [MPP][TFSI] ([MPP]: 1-methyl-3-propyl-pyrrolidinium).[49] The authors claimed that $[MPP]^+$ decomposition is related to reversible cation co-intercalation into the anode substrate, which was concluded from an increase in the step height on the HOPG surface.[49] Employing in situ atomic force microscopy (AFM), Shi and co-workers similarly suggested reversible cation co-intercalation into step edges of HOPG.[43] For more realistic battery materials, such as graphite composite electrodes consisting of KS6 graphite, Carbon SuperP, and polyvinylidene fluoride binder, it was found that $[TFSI]^-$ is too stable, hindering the formation of a SEI, which can support continuous cycling.[50] However, the formation of a passivation layer with SEI-like features was observed when cycling composite electrodes consisting of various graphite materials and binder in LiTFSI-containing [MPPp][TFSI] ([MPPp]: 1-methyl-1-propylpiperidinium).[44]

In the following, we first give a brief account of the experiments conducted at the graphite | [BMP][TFSI] + 0.1 M LiTFSI interphase during electrochemical cycling at different scan rates on i) well-defined, basal HOPG electrodes and ii) on binder-free graphite powder model electrodes, which are closer to realistic systems. By comparing the two model electrodes, we want to study the effect of the graphite structure on the IL decomposition/SEI formation. Ex situ X-ray photoelectron spectroscopy (XPS) was employed to compare the "chemical" SEI formed by vapor-deposition of multilayers of IL and subsequent Li post-deposition on the well-defined substrate in UHV to the "electrochemical" SEI formed during cyclic voltammetry (CV). Furthermore, depth profiling of the SEI was performed by Ar^+ sputtering; as well as sputtering of pure LiTFSI and [BMP][TFSI] to verify the influence of the Ar^+ beam.

Results and Discussion

Electrochemical characterization

First, we recorded cyclic voltammograms (CVs) on HOPG and on binder-free Mage graphite in LiTFSI-containing IL, which will be denoted as HOPG(Mage) | IL + LiTFSI, at different scan rates (potential range 1.5–0.02 V). Figure 1 depicts the first three cycles of the CVs recorded at 0.1 $mV\,s^{-1}$ (top) and the first cycle recorded on the same materials at 0.1, 1, and 10 $mV\,s^{-1}$ (bottom). Further cycles recorded at intermediate and fast scan rates are given in Figures S2 and S3 (see the Supporting Information). In the following, we will first discuss the potential range positive of 0.3 V and then the range 0.3–0.02 V.

Potential region from 1.5 to 0.3 V

Starting with CVs recorded on the basal HOPG substrate at slow scan rate (0.1 $mV\,s^{-1}$), the first cathodic scan shows a pre-peak at 0.7 V ($^{0.1}H_1$) and a maximum at 0.6 V ($^{0.1}H_2$; Figure 1a). For the CVs recorded at intermediate and fast scan rates, respectively (1 and 10 $mV\,s^{-1}$; Figure 1c and Figure S2), the peaks shift to lower potentials, namely to 0.6 ($^{1}H_1$) and finally to 0.4 V ($^{10}H_1$). No corresponding signals appear in the anodic scan above 0.3 V. These cathodic peaks disappear after the first cycle, regardless of the scan rate. Such behavior is typical for systems showing an irreversible surface passivation, as it was also observed for HOPG electrodes in organic electrolytes.[51,52] Accordingly, we assign the peaks to electrolyte decomposition, which results in self-poisoning for this process. Interestingly, a very similar peak is also observed in the CV of neat [BMP][TFSI] on HOPG (Figure 2), which indicates that the reductive decomposition process does not directly involve the Li^+ ion. However, the Li^+ cations (or possibly water) appear to enhance the electrolyte decomposition, as the current density is much higher when LiTFSI is added to the IL (which may also increase the resulting water content).

Previous results reported for HOPG-based systems are contradictory. Gasparotto and co-workers reported a rather fea-

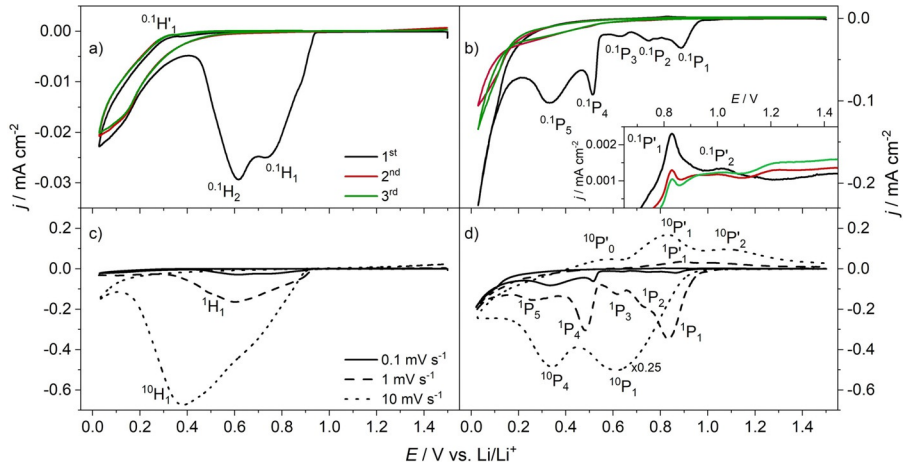

Figure 1. Cyclic voltammograms recorded on (a) HOPG and (b) Mage in [BMP][TFSI] + 0.1 M LiTFSI at 0.1 mV s^{-1} for three cycles, and the influence of the scan rate (10, 1, and 0.1 mV s^{-1}) during the first cycle on (c) HOPG and (d) Mage. The inset in (b) shows an enlarged part of the anodic scan(s). Peaks are marked H for HOPG and P for powder (Mage) electrodes, with indices for the scan speed (0.1, 1, 10 mV s^{-1}) and the peak number (in the order of their appearance). Anodic peaks are marked by an asterisk.

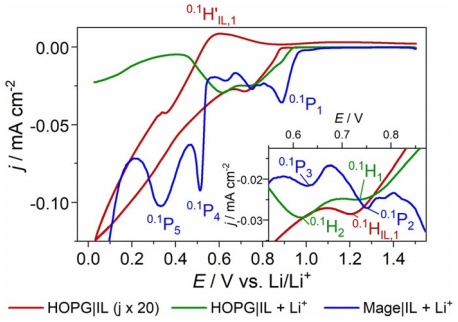

Figure 2. Comparison of the CVs (1st cycle) of HOPG in [BMP][TFSI] (red), HOPG in [BMP][TFSI] + 0.1 M LiTFSI (green), and Mage in [BMP][TFSI] + 0.1 M LiTFSI (blue) cycled at 0.1 mV s^{-1}. The inset shows the enlarged current traces in the reduction region between 0.9 and 0.5 V.

tureless CV in the first cycle for HOPG in 0.5 M LiTFSI-containing [BMP][TFSI] in the potential window of 1.0 to −2.0 V versus Pt[53] (about −1.5 to −4.5 V vs. Li/Li$^+$). Exploring the electrochemical properties of a HOPG electrode in [BMP][TFSI] + 0.5 M LiTFSI, Shi and co-workers observed a very small reduction peak at around 1.0 V in the cathodic scan, which, based on comparison with [BMP][FSI] (bis(fluorosulfonyl) imide anion), they assigned to reductive decomposition of [TFSI]$^-$.[43] Finally, also for a HOPG electrode but in [MPP][TFSI] + 0.5 M LiTFSI, Hu and co-workers reported a basically featureless CV (first scan) in the potential region between 1.5 and 0.3 V, with a minor reduction signal around 0.6 V. They, too, assigned the signal to reductive anion decomposition.[49]

The CVs recorded on the Mage powder electrodes appear more complex. When cycling at slow scan rate, we observe a cathodic peak already at 0.9 V ($^{0.1}P_1$). It behaves akin to the H_1 peak, shifting towards more negative potentials with increasing scan rate. Furthermore, it only appears in the first cycle. Therefore, we similarly assign it to a reductive, self-poisoning anion decomposition process leading to surface passivation for this process. The more positive reduction potential (peak maximum) compared with the HOPG substrate reflects the presence of more active sites on the graphite powder electrode compared with the HOPG substrate. Previous studies on binder-containing graphite compound electrodes reported that the reductive processes begin at 0.8 V in the cathodic scan, which was assigned to partly reversible [BMP]$^+$ intercalation.[44,54,55] Appetecchi and co-workers and Nádherná and co-workers both reported several irreversible reduction peaks between 0.8 and 0.3 V for graphite composite electrodes in [BMP][TFSI] in the first cathodic scan and more or less complete passivation of the surface towards further reductive reactions, although Li$^+$ (de)intercalation was still possible. They, too, assigned these peaks to cation co-intercalation, arguing that a) [TFSI]$^-$, compared with [FSI]$^-$, is too stable and hence does not decompose,[50] and that b) [FSI]$^-$ decomposition starts above 1.0 V and thus SEI formation takes place above the [BMP]$^+$ intercalation potential range.[56] However, these studies were conducted in dried electrolyte systems. It is therefore possible that the as-received electrolytes used by us undergo surface passivation owing to residual moisture/oxygen contamination. Moving on in the cathodic scan on our Mage powder electrode, a second peak (P_2) appears at about 0.7 V, that is, at the same potential as the $^{0.1}H_1$ peak, and a third peak (P_3) at about 0.6 V. Neither of them shifts when changing to an intermediate scan rate, indicating that they are due to (reversible) site-specific surface processes such as [BMP]$^+$ adsorption. At present, however, this cannot be specified further. Finally, two peaks appear at 0.5 (P_4) and 0.3 V (P_5) at slow and intermediate scan rates, which were not resolved on the HOPG electrode and thus seem to be characteristic for the graphite powder electrode. Changing to the fast scan rate, we find a P_1 peak at 0.6 V, which we assume corresponds to the down-shifted P_1 peak at slower scan rates, possibly together with the not or only slightly shifted P_2 and P_3 peaks. The next peak appears at 0.3 V, which we assume to correspond to the down-shifted P_4 at the slower scan rates, and we therefore denote it as $^{10}P_4$. There is no detectable analog to the P_5 peak at 10 mV s^{-1}. In-

terestingly, at the intermediate scan rate, the peak $^1P_4$ was detected over twenty cycles (Figure S3). The cathodic signals at lower potentials seem to be correlated with the anodic peaks at around 0.8–0.9 V (P'_1) and 1.0 V (P'_2) in the anodic scan at all scan rates, the current densities of which decrease in parallel with the current density of the signals P_4 and P_5. Thus, we suggest that these signals are due to (partly) reversible $[BMP]^+$ co-intercalation, in agreement with previous assignments.[56,57] It takes place in addition to increasing surface passivation, at least with respect to electrolyte decomposition (H_1/P_1). Our suggestion also agrees with the conclusions of an in situ Raman study by Markevich and co-workers, in which they assigned reduction signals between 0.7 and 0.5 V and around 0.3 V to cation co-intercalation and other ones around 0.8 and 0.2 V to irreversible $[TFSI]^-$ decomposition.[54]

Potential region from 0.3 to 0.02 V

Below about 0.3 V in the CV recorded on HOPG|IL + LiTFSI (Figure 1a,c), the reductive currents grow exponentially until the lower potential limit. The same applies for the CVs recorded on Mage in Li^+-containing ionic liquid (Figure 1b,d) and on HOPG in neat ionic liquid (Figure 2). Such an increase in reductive currents in Li^+-containing electrolyte at potentials below 0.2 V is usually attributed to Li^+ intercalation into graphite.[58] Although the intercalation of Li^+ into the basal plane of HOPG substrates is very slow,[59,60] it still may take place, for example, via step and edge defects on the surface.[34,54,61,62] In addition to Li^+ intercalation, the currents observed around 0.2 V have also been attributed both to $[TFSI]^-$ decomposition[54] and to $[BMP]^+$ intercalation as competing processes.[50,56] Furthermore, a subtle shoulder is present at approximately 0.3 V in the anodic scan on HOPG|IL + LiTFSI (peak H'_1; Figure S2), independent of the scan rate. At certain conditions (scan rate, cycle number), the net current at that peak is negative owing to the superposition with cathodic decomposition processes. Although a typical process in this potential region in the anodic scan would be Li^+ deintercalation, we favor an explanation where this peak arises from the re-oxidation of adsorbed decomposition products. This, we conclude from the appearance of a similar feature at 0.3 V in the CV recorded in Li-free electrolyte ($^{0.1}H'_{IL,1}$). The absence of Li^+ deintercalation seems to indicate that the concentration of defect sites on the HOPG electrodes is too low for significant contributions from Li^+ inter- and deintercalation.

As the concentration of defect sites on the Mage powder electrode is much higher than on the HOPG substrate, the currents starting at 0.2 V are more than ten times higher than the ones observed on HOPG. However, like on HOPG, no corresponding Li^+ deintercalation features appear in the anodic scan up to 0.3 V, where they have been observed in organic carbonate-based electrolytes on similar graphite compound electrodes.[44] It is worth noting that when studying the Li^+ intercalation behavior on composite KS6L graphite electrodes in different IL compositions, among them [BMP][TFSI] + 0.7 M LiTFSI, Nádherná and co-workers found Li^+ deintercalation peaks between 0.0 and 0.4 V in all of these electrolytes.[56] However, Appetecchi and co-workers, using composite KS6 graphite electrodes and [BMP][TFSI] + 0.3 M LiTFSI, observed only little and varying Li^+ (de)intercalation currents.[50] They attributed these variations to the inherent stability of $[TFSI]^-$ and the subsequently slower formation of a stable SEI. The latter was considered to be essential for reversible Li^+ intercalation, as it is observed for the less stable $[FSI]^-$.[50] Zheng and co-workers cycled natural graphite composite electrodes in [TMHA][TFSI] + 1 M LiTFSI ([TMHA]: trimethyl-*n*-hexylammonium).[63] They, too, observed only minor Li^+ (de)intercalation. However, both the cathodic and the anodic current densities around 0 V increased with increasing cycling time, whereas the (supposed) IL cation co-intercalation currents at higher potentials decreased. This is particularly the case after the addition of SEI-forming additives, such as vinylene carbonate.[63]

We agree with the above-mentioned report that the processes taking place in [BMP][TFSI] (+ LiTFSI) on our model substrates do not lead to the formation of a functional SEI layer. We suggest that two catalytic electrolyte decomposition processes are at play: one at potentials above 0.3 V, which is rapidly inhibited, and another one occurring at potentials below 0.3 V, which is not necessarily affected by this self-poisoning process and continues for several cycles. It is not clear if, especially on the graphite powder electrode, the latter process is also accompanied by Li^+ or $[BMP]^+$ intercalation and whether it results in the formation of a surface layer that passivates against further insertion processes. In recent differential electrochemical mass spectrometry (DEMS) studies, we found indirect evidence for the formation of adsorbed decomposition products in Li^+-containing [BMP][TFSI].[47] This was concluded from the lack of volatile decomposition products during the reduction in Li^+-containing electrolyte, whereas $[BMP]^+$ and $[TFSI]^-$ fragments were found in neat and Mg^{2+}-containing IL.[47]

XPS characterization

To gain a more detailed understanding of the formation and composition of this passivation layer, we employed X-ray photoelectron spectroscopy for the characterization of additional model systems. Beginning with a well-defined, UHV-prepared model system, we first studied the effect of Li post-deposition on a multilayer film of [BMP][TFSI], which was pre-deposited under UHV conditions on a HOPG substrate. In addition, we also recorded detail spectra from a LiTFSI powder sample as reference. Next, we characterized a HOPG working electrode, which was exposed to [BMP][TFSI] + 0.1 M LiTFSI at open circuit potential (OCP) for 68 h. In a third step, we studied a similar electrode and a Mage powder electrode after the potential cycling discussed in the previous section. Finally, sputtering of LiTFSI salt as well as depth profiling experiments of the HOPG sample after immersion into the IL at the OCP and of the electrochemically cycled graphite electrodes (both HOPG and Mage) were conducted by using Ar^+ sputtering.

Comparison: a chemically and an electrochemically formed SEI

In Figure 3, we compare the XP core level spectra of the F 1s, Li 1s, O 1s, N 1s, C 1s, and S 2p regions of the SEI formed on the HOPG substrate after vapor deposition of a [BMP][TFSI] multilayer film (10 ML, ML = monolayer; Figure 3 a), after subsequent Li deposition (Figure 3 b) under UHV conditions, and of the SEI formed electrochemically on the HOPG and Mage substrates by potential cycling in a 0.1 M LiTFSI-containing [BMP][TFSI] electrolyte (Figure 3 e, f). XP reference spectra of LiTFSI (Li salt) and of the 0.1 M LiTFSI in [BMP][TFSI] electrolyte are also displayed (Figure 3 c, d).

We begin by briefly describing the characteristic XP spectra of the [BMP][TFSI] multilayer film deposited on HOPG under UHV conditions (Figure 3 a), which will be used as reference spectra for the following experiments. In the detail spectra of the different regions, all $[TFSI]^-$-related peaks are colored blue and all $[BMP]^+$-related ones red. In the F 1s spectrum, a single peak appears at 689.5 eV, originating from the F atoms of the $-CF_3$ group in the $[TFSI]^-$ anion (F_{TFSI}). The O 1s spectrum shows a peak at 533.3 eV, which is related to the $[TFSI]^-$ sulfonyl groups (O_{TFSI}). Two well-separated peaks in the N 1s spectrum at 403.3 and 400.0 eV represent the nitrogen atoms within the pyrrolidinium cation (N_{BMP}) and the imide anion (N_{TFSI}), respectively. Their intensities show a 1:1 ratio of N_{BMP}/N_{TFSI}, as expected for molecularly adsorbed [BMP][TFSI] species. In the C 1s region, the signal at 293.5 eV is assigned to the $-CF_3$ group (C_{TFSI}) of the $[TFSI]^-$ anion, whereas the ones at 287.3 eV and 286.0 eV, respectively, represent the carbon bonded to nitrogen (C_{hetero}) and the alkyl-type carbon atoms (C_{alkyl}) of the $[BMP]^+$ cation. Similar to the N 1s region, the C 1s spectrum reflects molecularly adsorbed [BMP][TFSI] with a peak area ratio $C_{TFSI}/C_{hetero}/C_{alkyl}$ of 1.8:4.3:5, in agreement with the nominal atomic ratio of 2:4:5 in [BMP][TFSI]. A low-intensity shoulder at 284.6 eV is due to the underlying graphite sub-

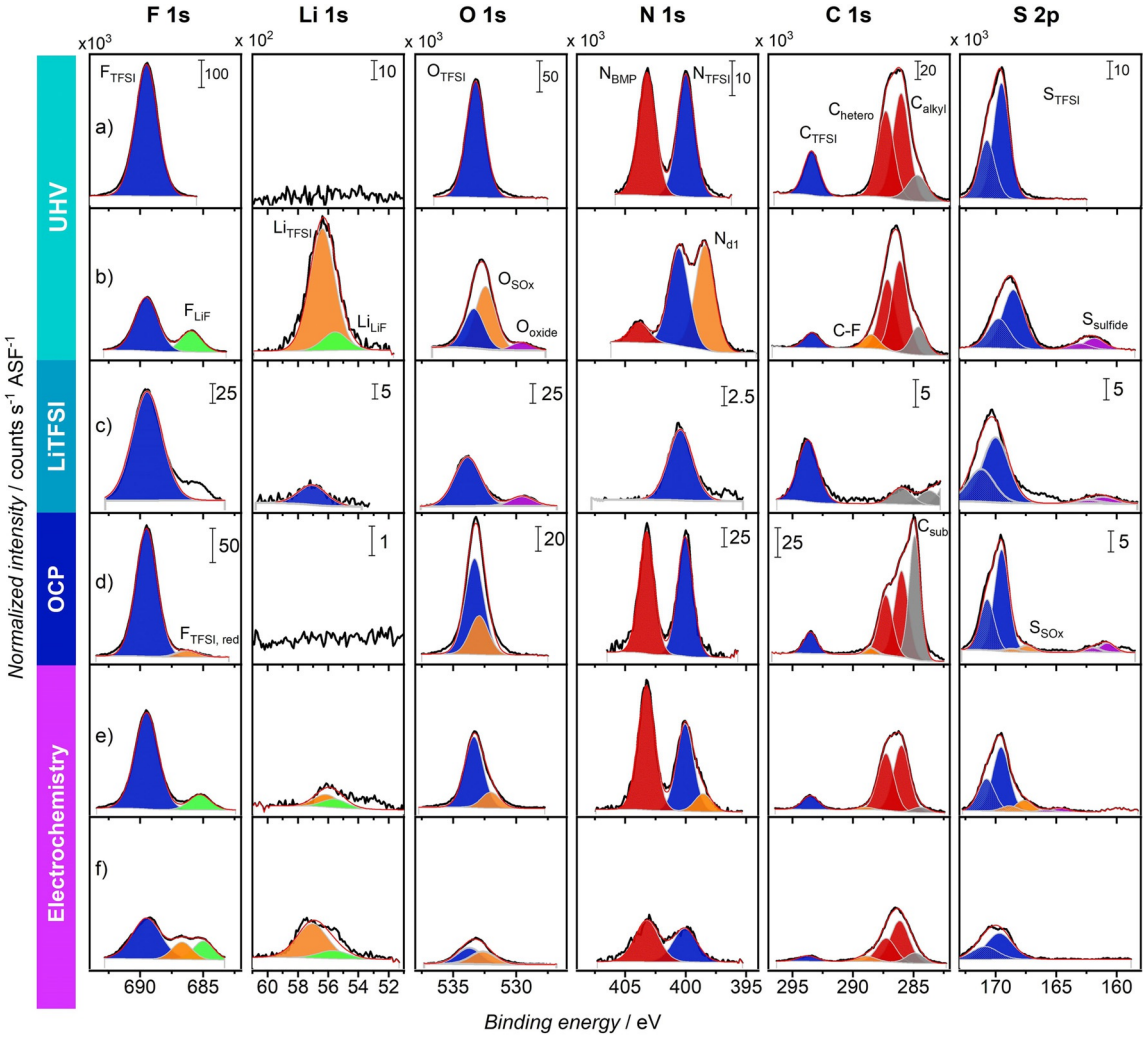

Figure 3. Core-level spectra of the SEI formed on HOPG by vapor deposition under UHV conditions (a, b), of neat LiTFSI (c), of the surface layer formed on HOPG in LiTFSI-containing [BMP][TFSI] held at OCP (d), and of the SEI formed electrochemically on HOPG and Mage (e, f). In detail: XP spectra of (a) a 10 ML film of [BMP][TFSI] on HOPG prepared by vapor deposition, (b) the same film after subsequent deposition of Li, (c) LiTFSI salt for reference, (d) a HOPG electrode held at OCP in [BMP][TFSI] + 0.1 M LiTFSI, and the SEI formed on HOPG (e) and on Mage (f) by potential cycling in [BMP][TFSI] + 0.1 M LiTFSI. The intensity scales given in (d) apply to (e) and (f), as well. Larger versions of these spectra are given in the Supporting Information.

strate (C_{sub}, filled gray),[64] which is strongly damped by the IL multilayer film. In the S 2p region, finally, a doublet for the $-SO_2CF_3$ species (S_{TFSI}) appears at 169.6 ($S\,2p_{3/2}$) and 170.8 eV ($S\,2p_{1/2}$). Our assignment is in agreement with those reported previously for [BMP][TFSI] on metal (oxide)[28–30,32,33,39] and HOPG substrates,[28,36] as well as for similar ionic liquids containing $[TFSI]^-$ anions on Au(111).[65]

In the next step (Figure 3b), Li (≈3 monolayer equivalents, MLEs) was post-deposited on the substrate covered by 10 ML of IL at room temperature. The $[BMP]^+$- and $[TFSI]^-$-related peaks (F_{TFSI}, O_{TFSI}, N_{BMP}, C_{TFSI}, S_{TFSI}, C_{hetero}, C_{alkyl}) decreased in intensity after the Li deposition step, indicating both partial cation and anion decomposition and/or desorption. At the same time, new peaks arise (filled orange) in the Li 1s, N 1s, C 1s, and S 2p spectral ranges, which must be due to the formation of decomposition products. However, the losses in intensity differ not only between cation- and anion-related peaks, but also between different signals assigned to either anion (or cation) decomposition. Two exemplary cases are i) the N_{BMP} and corresponding N_{TFSI} peaks, which show a pronounced difference in intensity loss, and ii) the difference between N_{TFSI} and F_{TFSI} or C_{TFSI} peaks, where the decrease in the first one is much smaller than that in the latter ones. A quantitative discussion of the rather different trends in peak intensities will be given below.

First, after Li deposition, the F_{TFSI}, O_{TFSI}, and C_{TFSI} peaks all decrease by about 60–65%. The F_{TFSI}/C_{TFSI} ratio, which is 3:1 for $[TFSI]^-$, changes to 3.3:1, indicating a loss of the C component compared with the F component, even though they both originate from the $-CF_3$ groups of the anion. This discrepancy may be explained by the formation of new, fluorine-containing moieties, such as C–F species (C 1s: 290–287 eV[64]). This would be plausible, as they appear at an almost identical binding energy (BE) in the F 1s range as $-CF_3$, but at a significantly lower BE in the C 1s range. The transformation from $-CF_3$ to C–F is supported by the appearance of a new C 1s peak with low intensity at 288.5 eV (C–F, filled orange). The sum of the F 1s intensities of the C–F and $-CF_3$ peaks indeed accounts for the intensity of the F_{TFSI} peak in the F 1s region (within the error margins given by the atomic sensitivity factors (ASFs)). At the same time, a new peak appears at 685.8 eV in the F 1s spectrum (F_{LiF}, filled green), which we attribute to LiF.[32,64] Such a peak was recently obtained also upon stepwise deposition of Li onto an adsorbed IL (sub)monolayer on HOPG under UHV conditions, where details about the decomposition mechanism were revealed by a combined computational analysis.[34] The formation of LiF as decomposition product is also in excellent agreement with ab initio molecular dynamic simulations by Ando and coworkers,[66] which included electric field effects. These authors predicted that $[TFSI]^-$ is reduced on a lithium electrode independently of the applied potential. Briefly, $[TFSI]^-$ interaction with the Li electrode results in cleavage of the S–C and C–F bonds and the subsequent formation of LiF. Furthermore, XP spectra recorded after electrochemical measurements of an IL containing $[TFSI]^-$ anions and a Li salt also obtained LiF.[48] Its appearance in our measurements is also confirmed by a corresponding signal at 55.9 eV (filled green) in the Li 1s spectrum,[64] the intensity of which corresponds to a 1:1 atomic ratio of Li/F. The remaining peak area of the Li 1s signal is filled by an additional peak at 56.4 eV (filled orange), which is most likely due to other Li-containing decomposition products or LiTFSI. All in all, we observe a loss of about 45% of the total intensity in the F 1s spectrum, which probably is due to the formation and desorption of volatile decomposition products. The O 1s spectrum obtained after Li post-deposition is characterized by three peaks, which are obtained by fixing the BE position of the O_{TFSI} peak at 533.3 eV and leaving the rest of the spectrum to be filled by two further peaks. The nominal O_{TFSI}/F_{TFSI} ratio of the first peak is approximately 3.7:6, indicating a decrease of the O_{TFSI} species by 63% compared with before Li deposition. This agrees well with the similar intensity decrease in the F_{TFSI} and C_{TFSI} peaks, respectively, after Li deposition. The new O 1s peaks appearing at 532.4 eV (filled orange) and at 529.6 eV (filled violet) are characteristic of sulfite and oxide species (O_{SOx} and O_{oxide}, respectively).[64] Howlett and co-workers reported the formation of sulfite species (e.g., Li_2SO_3) in the SEI formed on a Li metal electrode after galvanostatic cycling in $[TFSI]^-$-based electrolyte and subsequent XPS characterization.[39] Differently than the F 1s region, the total sum of the intensity in the O 1s spectrum does not decrease upon Li post-deposition, indicating that the volatile decomposition products are essentially free of oxygen. The N 1s spectrum after Li post-deposition features a shift of the two main peaks by 0.6 eV towards higher BEs, and a new signal appears at the lower BE side (N_{d1}, filled orange). The N_{TFSI} peak shows a very low intensity decrease of only 10%, which is in contrast to the considerable intensity loss of all other anion-related peaks in the other spectral ranges by around 60%. Hence, we assume that the decline of the N_{TFSI} signal is compensated by the formation of (Li-bound) decomposition products of $[TFSI]^-$, such as $LiNSO_2CF_3$,[34] which have a rather similar N 1s BE as $[TFSI]^-$. Interestingly, the cation peak intensity loss is much more pronounced than that of the N_{TFSI} peak (about 80%), indicating that most of the cations are decomposed and that the extent of $[BMP]^+$ decomposition even exceeds that of $[TFSI]^-$ decomposition. The new peak at 398.4 eV has been ascribed to Li_3N[32,39,67–69] although other nitrogen-containing Li-bound fragments, for example, linear LiC_xH_yN species resulting from a ring-opening of the pyrrolidinium molecule,[34,70] might be possible as well. Despite the strong changes in the individual peak intensities, however, the total peak intensity of the N 1s spectrum remains almost constant, similar to that in the O 1s region, but different from the F 1s signal. In the C 1s range, the shape of the spectrum changes significantly after Li deposition, now showing a much more pronounced maximum between 284.0 and 287.0 eV, indicative of changes of the $C_{TFSI}/C_{alkyl}/C_{hetero}$ ratio. As discussed above, the C_{TFSI} peak decreases by 64%, which is plausible considering the similar decrease of the F_{TFSI} and O_{TFSI} peak intensities observed in the respective BE regions. However, the loss indicated in the N 1s spectrum for the $[BMP]^+$ species (about 80%) is not reflected in the loss of the peak intensities of the C_{hetero} and C_{alkyl} peaks at 287.3 eV and 286.0 eV, respectively, of 20 to 30%. We suggest that the apparent 'excess' of C–H species in the C 1s region is due to the formation of $[BMP]^+$ decomposition products with similar func-

tional groups and thus similar BEs, resulting in a total loss of 21% in the ASF-normalized intensity for the C 1s region after Li post-deposition. Next, in the S 2p BE region, the doublet for S_{TFSI} decreases in intensity by approximately 27% and the shape of the signal broadens towards lower BEs, implying the presence of anion decomposition products with very similar BEs. Simultaneously, the C_{TFSI}/S_{TFSI} ratio of 1:1 for intact $[TFSI]^-$ changes to around 1:2 after Li post-deposition. Again, judging from the F_{TFSI}, O_{TFSI}, and C_{TFSI} signals, the intensity of the S 2p S_{TFSI} doublet should decrease by about 60–65%. However, the loss caused by Li post-deposition in the S 2p spectral range is only about 27%. We attribute this discrepancy to the formation of S-containing $[TFSI]^-$ decomposition products with similar BEs as the anion. Buchner and co-workers have discussed the possibility of the formation of sulfite species, for example, Li_xSO_y, upon the post-deposition of Li on pre-adsorbed [BMP][TFSI] adlayers on Cu, which resulted in the appearance of a S $2p_{3/2}$ doublet at around 166.2 eV.[32] This is in agreement with the doublet observed at around 167.5/168.7 eV in our work, and with the results obtained by Howlett and co-workers.[39] We are, however, unable to distinguish between different sulfite species such as $Li_2S_2O_4^-$, Li_2SO_3, $LiSO_2CF_3$, etc. from the present XP spectra. The sulfite contribution also agrees with the presence of the O_{SOx} signal in the O 1s spectrum, as the ratio of $(O_{SOx}+O_{TFSI})$ to S_{TFSI} is around 2.6, which would be in agreement with a mixture of $[TFSI]^-$ and SO_x species. In addition, a new doublet is observed at 161.8/163.0 eV (filled violet). This, we tentatively attribute to polysulfides[68] or Li_2S species.[32] The overall loss of intensity upon Li post-deposition on IL adlayers in the S 2p spectrum is only 13%, indicating both the loss of $[TFSI]^-$ and the formation of S-containing product species. Finally, for the Li 1s region, we see a pronounced peak upon Li post-deposition, resulting in a concentration of almost 25%. Furthermore, we can cross-check the consistency of the above signal assignments. Assuming the formation of LiF (F 1s peak at 686.0 eV), Li_2O (O 1s peak at 529.6 eV), Li_3N (N 1s peak at 398.0 eV), $LiCF_x$ (C 1s peak at 288.5 eV), Li_2S (S 2p peak at 161.8 eV), and LiTFSI (or Li-bound $[TFSI]^-$ fragments, e.g., $LiNSO_2CF_3$, the contribution of which is calculated as the difference between the N_{BMP} and the N_{TFSI} peak intensities at 403.3 and 400.0 eV) as the Li-containing species, these can account for 88% of the total Li 1s peak intensity, underlining the credibility of our peak assignments.

In the following, we briefly discuss the XP spectra recorded for the LiTFSI powder. In the spectra shown in Figure 3c, we find all peaks (F_{LiTFSI}, O_{LiTFSI}, N_{LiTFSI}, C_{LiTFSI}, S_{LiTFSI}, Li_{LiTFSI}) expected for $[TFSI]^-$-containing species. Interestingly, all BEs of the LiTFSI-related peaks are up-shifted by around 3 eV compared with those in [BMP][TFSI]. The massive up-shift points toward a positive charging of the sample surface, indicative of a rather low electrical conductivity. Even after that correction there are slight variations in the BE compared with the [BMP][TFSI] multilayer film, which we tentatively attribute to the influence of the different cation (Li^+ instead of $[BMP]^+$).[32] In addition, all peaks are slightly broadened in comparison to the peaks shown in Figure 3a, b, which we assign to differential and non-uniform charging effects. Finally, the O 1s spectrum reveals an additional peak at 529.4 eV (O_{oxide}, filled violet), which we assign to oxygen-containing contaminations of the LiTFSI salt.

Next, we move on to the XP spectra of the HOPG sample kept in the IL + 0.1 M LiTFSI electrolyte in the electrochemical cell at open circuit conditions (OCP) for 68 h (HOPG|IL@OCP). This way, we wanted to test for the influence of the Li counter and reference electrodes on the SEI formation. XP spectra recorded subsequently, after rinsing the sample with dimethyl carbonate (DMC) and subsequent transfer into the UHV chamber without contact to air, are depicted in Figure 3d. The spectra are rather similar to those obtained for [BMP][TFSI] multilayer films deposited under UHV conditions, with their F_{TFSI}, O_{TFSI}, N_{TFSI}, C_{TFSI}, C_{hetero}, C_{alkyl} and S_{TFSI} peaks, respectively (see Figure 3a). Clearly, small amounts of IL remained on the HOPG surface after rinsing. Only the C 1s spectrum contains a slightly higher contribution of the graphitic substrate (C_{sub}) than in Figure 3a, indicative of a thinner or inhomogeneous IL layer remaining on the HOPG substrate compared with the 10 ML film in Figure 3a (1 ML ≈ 0.3 nm). The quantitative evaluation reveals a N_{BMP}/N_{TFSI} ratio of 1:1, as expected for molecularly adsorbed [BMP][TFSI] species. However, the C 1s intensity ratio of $C_{TFSI}/C_{hetero}/C_{alkyl}$ of 1:3:5 instead of 2:4:5 suggests that some cation decomposition has taken place where the C–N- and C–H-containing decomposition products are superimposed with the C_{hetero} and the C_{alkyl} signals. A slight C 1s deficiency is observed also for the anions based on a number of peak intensity ratios, including the F_{TFSI}/C_{TFSI} ratio (4:1 instead of 3:1), the S_{TFSI}/C_{TFSI} ratio (1.1:1), the O_{TFSI}/C_{TFSI} ratio (2.55:1), and the N_{TFSI}/C_{TFSI} ratio (0.64:1). The low-intensity C–F peak at 288.5 eV in the C 1s spectrum also points towards $[TFSI]^-$ decomposition, possibly caused by the metallic Li counter and reference electrodes. Interestingly, we obtained no signal in the Li 1s spectrum, although we used LiTFSI-containing electrolyte. However, considering that there are about 30 $[BMP]^+$ ($[TFSI]^-$) ions for every single Li^+ ion, and thus 180 F atoms for each Li^+ in the electrolyte, and taking into account also the low ASF of the Li 1s peak, this would not be expected. As an example, if there is no enrichment of Li on the surface, the F peak must be approximately 15000 times higher than the Li peak. With a total of about 440000 counts (normalized intensity), the Li signal would be about 29 counts and thus is entirely lost in the noise.

Finally, we discuss the XP core-level spectra of the electrochemical SEI, which is formed by potential cycling on HOPG (HOPG|SEI) and on Mage (Mage|SEI) electrodes. The resulting spectra are presented in Figure 3e, f. The spectra of the SEI formed on HOPG during potential cycling largely show intact, adsorbed IL species, which remained on the surface after rinsing, together with small amounts of decomposition products (filled orange): decomposed $[TFSI]^-$ species at approximately 688 eV (F 1s) and 398 eV (N 1s), SO_x at 533 eV (O 1s), and 167 eV (S 2p), and C_{C-F} at 288.5 eV (C 1s). In the F 1s BE region, specifically, we find a LiF peak at 685.0 eV (filled green and down-shifted by 0.8 eV from the position observed for sample b). The corresponding Li_{LiF} peak appears at 55.6 eV in the Li 1s spectrum. As observed and discussed with the sample characterized after Li post-deposition on a UHV-prepared IL film (sam-

ple b), we find a higher relative intensity loss of the C_{TFSI} peak compared with the F_{TFSI} and N_{TFSI} peaks. Both in the N 1s and the C 1s spectrum, the ratio of the intensities of the $[TFSI]^-$ peaks and the $[BMP]^+$ peaks decreases in comparison to the pristine IL, that is, the intensity of the $[TFSI]^-$ peak has decreased. It appears that $[TFSI]^-$ decomposition takes place preferentially during electrochemical SEI formation. These results agree well with our CV experiments reported above; as well as with numerous studies claiming reductive $[TFSI]^-$ decomposition.[38,39,42,43,45,46,48,49,71,72] In contrast, $[BMP]^+$ is predominantly decomposed under surface science conditions, that is, upon post-deposition of Li on a multilayer film of the IL. Preferential cation decomposition ($[BMP]^+$ and $[OMIm]^+$ ([OMIm]: 1-octyl-3-methylimidazolium), respectively) on Li layers and after Li post-deposition has also been reported previously.[32,70] However, of all BE regions, the C 1s range is the one least suited for the (quantitative) interpretation of possible products, as it—except for the C–F peak—only features the characteristic IL and substrate peaks. Any possible decomposition products would be superimposed by the original signals, as was discussed above. In addition, the graphite C_{sub} peak is comparatively low, demonstrating that a film with a thickness of >6–9 nm must cover the HOPG surface. The Mage|SEI sample displays most of the features characteristic for the HOPG|SEI sample. In addition, a third F 1s signal for reductively decomposed $[TFSI]^-$ species with about similar intensity as the LiF peak appears in between the F_{TFSI} and the F_{LiF} signal (286.7 eV). In the Li 1s spectrum, there is a pronounced intensity at a BE higher than LiF. This could either be due to LiTFSI or related decomposition products. Furthermore, the peaks observed for the SEI formed on the Mage substrate are strongly broadened owing to differential charging. However, the wide peak shape could also be related to the presence of products with different oxidation states.

Effect of Ar^+ sputtering on the SEI

To gain deeper insight into the possibly varying composition during electrochemical SEI growth, we recorded depth profiles, characterizing the surface composition of the SEI after different times of Ar^+ sputtering. Here, it is important to note, however, that sputtering will in any case result in a roughening of the surface. Furthermore, the composition detected by XPS after certain sputter times will not be exactly identical to that of the original SEI at the corresponding level owing to the selective element removal caused by different sputter yields, and sputter-induced decomposition of the molecules present in the film may lead to additional changes. To test for such effects, we first carried out Ar^+ sputtering of pure LiTFSI salt (Figure 4). Here, we minimized the measurement time by recording only F 1s and Li 1s detail spectra, which showed the largest changes in the other sputter experiments described below. The results will be used as the basis for the interpretation of the XP spectra obtained from a SEI layer formed on HOPG under OCP conditions (Figure 4) and of a SEI formed by potentiodynamic cycling on HOPG and Mage electrodes (Figure 5).

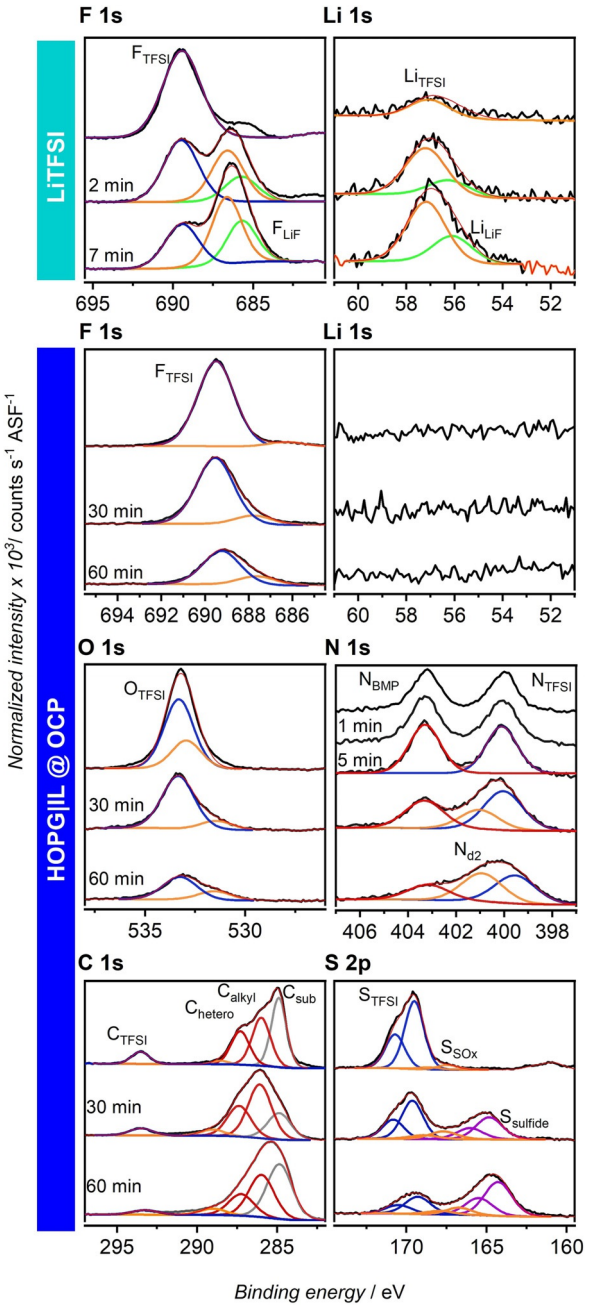

Figure 4. Top: F 1s and Li 1s core level spectra of LiTFSI before and after stepwise Ar^+ sputtering (after 2 and 7 min of successive sputtering). Bottom: F 1s, Li 1s, O 1s, N 1s, C 1s, and S 2p core-level spectra of sample c (HOPG at OCP in [BMP][TFSI] + 0.1 M LiTFSI for 68 h) recorded after in total 30 and 60 min of successive sputtering (for N 1s: additional data after 1 and 5 min of sputtering).

Starting with the reference spectra recorded upon LiTFSI sputtering, the F 1s region shows a decay in intensity of the F_{TFSI} (blue line) peak at 689.5 eV after 2 min of sputtering compared with the situation before sputtering (see Figure 3c). Furthermore, two new peaks arise at 686.7 and 685.7 eV, pointing to sputter-induced $[TFSI]^-$ decomposition. The new peaks are assigned to decomposition products such as $LiNSO_2CF_3$ or other C–F species ($F_{TFSI,red}$, see discussion above) and LiF (F_{LiF}),

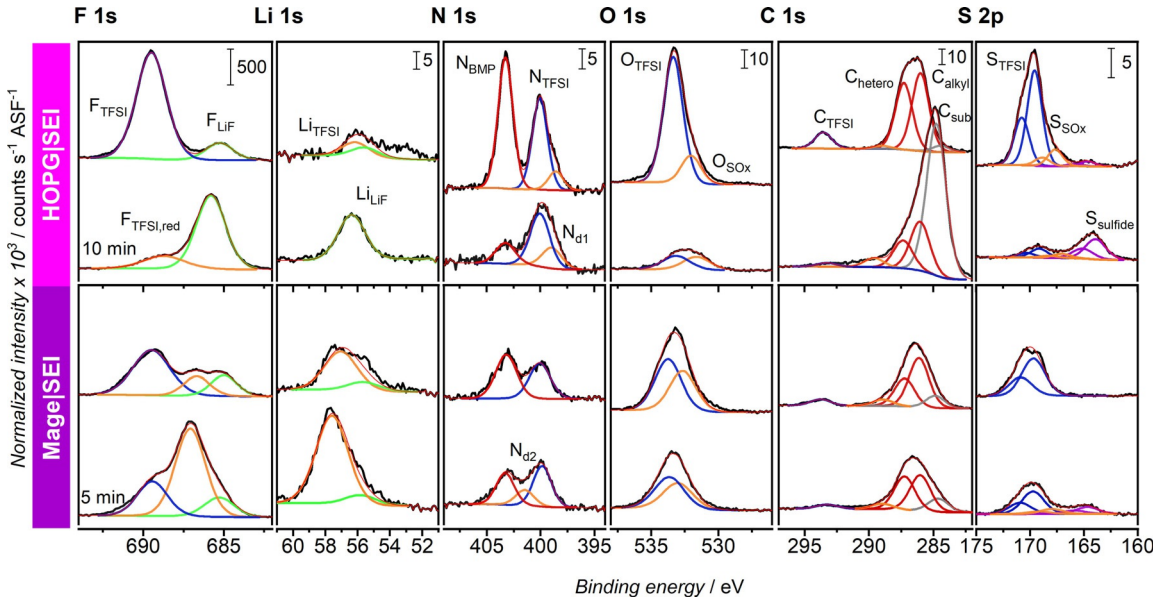

Figure 5. Core-level spectra of the SEI formed electrochemically on HOPG (sample e) and Mage (sample f) before and after 10 (5) min of Ar^+ sputtering. Note that the spectra recorded before sputtering are identical with those shown in Figure 3.

respectively. This trend continues for increasing sputtering time. Correspondingly, the signals in the Li 1s range are associated with $[TFSI]^-$ and reduced $[TFSI]^-$, as well as LiF. Note that the Li 1s peaks for Li_{TFSI} and $Li_{TFSI,red}$ cannot be distinguished in the fit and are assigned to the signal at 57.0 eV, whereas the Li_{LiF} signal appears at approximately 56 eV. Overall, Ar^+ sputtering of pristine LiTFSI clearly demonstrates decomposition of $[TFSI]^-$ to sputter-induced $[TFSI]^-_{red}$ moieties and other decomposition products, as well as LiF.

Similar XPS measurements were performed on the sample HOPG | IL@OCP. The XP spectra of the F 1s, O 1s, N 1s, C 1s, and S 2p regions recorded before sputtering are dominated by the $[BMP]^+$ and $[TFSI]^-$ characteristic peaks discussed with Figure 3 d.

Interestingly, the N 1s region reveals no sputtering-induced changes after 1 and 5 min of sputtering, except for an increase in total N 1s intensity. The latter may be due to sputter-removal of other species. Most important, the intensity ratio of the N_{TFSI} and N_{BMP} peaks in the N 1s spectrum is essentially constant during this time, indicating that the adlayer is still dominated by molecular [BMP][TFSI] species (Figure 4, panel at the bottom, left) after 5 min of sputtering. Upon increasing the sputtering time to 30 min and then to 60 min in total, we observed changes in the F 1s, O 1s, N 1s, C 1s, and S 2p regions. Now, the F 1s peak area decreased stepwise in intensity, and a low-intensity peak appears at the lower BE side (yellow line, 687.5 eV), which we assign to a small amount of sputter-induced $[TFSI]^-$ decomposition products. If sputtering results in the removal of fluorine atoms, this would result in volatile C–F_2 and C–F species, which may be bound to N or SO_x moieties (see discussion below). However, the changes observed in the F 1s region of the HOPG | IL@OCP sample after 30 min of sputtering are minor compared with the ones occurring after already 2 min of sputtering of the LiTFSI sample. Clearly, LiTFSI undergoes a more pronounced sputter-induced decomposition than [BMP][TFSI] itself.

Furthermore, the presence of Li strongly affects the sputter decomposition of $[TFSI]^-$, leading mainly to LiF formation. Based on force–distance atomic force[73] and quartz microbalance measurements,[48] it has been concluded that Li^+ cations result in a destabilization of $[TFSI]^-$ by influencing the electrochemical double layer formed on the substrate. According to these authors, Li^+ leads to formation of $[Li(TFSI)_2]^-$ complexes, which increases the concentration of $[TFSI]^-$ moieties at the anode and enhances anion decomposition. Overall, the concentration of LiTFSI is crucial for the coordination process,[74] and for $[TFSI]^-$ decomposition. No signal was observed in the Li 1s region, as expected from the low cross-section of Li 1s and the low concentration (as discussed with Figure 3). Moving on, the O 1s range is dominated by the O_{TFSI} peak at around 533.3 eV (blue line), which decreases in intensity upon increasing sputtering time. After 30 and 60 min of sputtering, a second peak appears at 531.6 eV, indicative of the formation of sputter-induced $[TFSI]^-$ decomposition products (O_{SOx}, yellow line). The main change in the spectra is, however, the decrease in the total peak area of both the F 1s and the O 1s peaks, pointing to a loss of fluoride- and oxygen-containing species in the accessible film region. In the N 1s range, 60 min of sputtering finally resulted in a decrease of the $[BMP]^+$ and the $[TFSI]^-$ peaks appearing at 403.3 and 400.0 eV in the original SEI layer. The loss is particularly pronounced for the N_{BMP} peak. This points to the onset of sputter-induced IL decomposition, which mainly affects the $[BMP]^+$ cation and less the $[TFSI]^-$ anion. Among the decomposition products is a nitrogen-containing species with an N 1s BE of around 401 eV (N_{d2}, yellow line), which appears after 30 min of sputtering and increases with continued sputtering. As the BE of this signal is located between those of the negative $[TFSI]^-$ and the positive

$[BMP]^+$ N 1s signals, we assign it to a covalently bound nitrogen atom in an uncharged moiety. Based on the BE, *N*,*N*-dibutyl-*N*-methylamine or methylpyrrolidine (N–C) would be possible candidates. For the C 1s region, we observed a distinct increase in intensity for longer sputter times, dominated by a broad peak around 285 eV (C_{hetero}, C_{alkyl}, C_{sub}). At the same time, the C_{TFSI} signal decreased, in agreement with the decrease of the anion-related signals in all other BE regions. Finally, in the S 2p region, two new doublets emerge with BEs of 164.3 and 166.7 eV for the S $2p_{3/2}$ peaks (yellow lines), respectively. The intensity of these doublets is, however, very low. The latter doublet (S $2p_{3/2}$: 166.7 eV) may be related to sulfur-containing decomposition products like Li_xSO_y, as discussed above, whereas the former one (S $2p_{3/2}$: 164.3 eV) is assigned to sulfide species (Li_2S). Quantitatively, the S_{SOx}/O_{TFSI} ratio is between 1:2 and 1:3, which would be in good agreement with Li_2SO_2 or Li_2SO_3 species. Moreover, the total intensity for the S 2p peaks is about constant during sputtering. Overall, the XP spectra during stepwise sputtering of [BMP][TFSI] indicate the selective desorption of F- and O-containing fragments or atoms, whereas the Li-, N-, and S-containing decomposition products of $[BMP]^+$ and $[TFSI]^-$, such as $Li_xC_yH_zN$, *N*,*N*-dibutyl-*N*-methylamine or methylpyrrolidine, Li_xSO_y, or Li_2S, remain on the surface. Both in LiTFSI and in [BMP][TFSI], however, the $[TFSI]^-$ anions undergo decomposition upon Ar^+ sputtering, with the decomposition products similar to those obtained in the SEI upon electrochemical reduction. In that sense, the results of depth profiling measurements of the SEI have to be taken with care.

Next, we performed depth profiling of the SEIs formed after the electrochemical measurements. The XP core-level spectra recorded before and after 10 (5) min of sputtering on the HOPG and Mage electrodes, respectively, are shown in Figure 5. To begin with, the HOPG | SEI surface before sputtering (top of each panel) features F_{TFSI}, O_{TFSI}, N_{BMP}, and N_{TFSI}, C_{TFSI}, C_{hetero}, C_{alkyl}, and S_{TFSI} peaks, as well as peaks related to decomposition products, which were already discussed together with the data in Figure 3. They include, for example, $[TFSI]^-$ decomposition products like $LiNSO_2CF_3$ and C–F moieties (yellow lines) in the F 1s region, Li_3N in the N 1s region (yellow lines), Li_xSO_y (yellow lines), and Li_2S (violet line of almost negligible intensity) in the S 2p region, as well as LiF (green line) in the F 1s and Li 1s regions.

After 10 min of Ar^+ sputtering, the F_{TFSI} peak in the F 1s range has disappeared almost completely. At the same time, a new, dominant signal arises at the low BE side, which, based on its BE, is attributed to LiF (green line). The related Li 1s peak appears at around 56 eV. Interestingly, the characteristics observed for the sputtered SEI on HOPG are almost identical to those of pristine LiTFSI after sputtering (Figure 4, top panels), but are in contrast to the traits observed after sputtering of the HOPG | IL@OCP sample (Figure 4, lower panels). This discrepancy seems to indicate that LiTFSI is enriched in the SEI formed upon potential cycling and that LiF formation is subsequently induced by the Ar^+ beam. However, we cannot rule out that LiF results directly from electrochemical $[TFSI]^-$ decomposition, and thus is a natural part of the SEI in regions closer to the electrode | electrolyte interface. For the HOPG | SEI sample, the N_{d1} peak (Li_3N, etc.) at 398.0 eV increases upon sputtering, whereas, for the Mage | SEI sample, a new peak (N_{d2}) appears at about 401.1 eV (N–C, etc.). This peak was observed already for HOPG | IL@OCP after 30 min of sputtering and was assigned to neutral, N-containing $[TFSI]^-$ decomposition products. We tentatively suggest that the N_{d2} peak-related decomposition product arises from sputtering of the IL, as it is only observed after sputtering. The O 1s spectra resemble the sequence of spectra obtained upon sputtering of the HOPG | IL@OCP sample, revealing desorption of oxygen-containing species. In the C 1s region, the anion-related C_{TFSI} peak also disappears almost completely, whereas the $[BMP]^+$-related C 1s peaks decrease in intensity but do not disappear completely. In contrast, the C_{sub} peak strongly increases, as expected upon sputter removal of part of the SEI layer. We suggest that most likely the $[BMP]^+$ species is partly transformed into other nitrogen- and carbon-containing species (N–C species, see N 1s region). Finally, the S_{TFSI}-related peak disappeared almost completely. As the O_{TFSI} and C_{TFSI} peaks decrease, as well, we conclude that the $[TFSI]^-$ species are either desorbed and/or sputter-transformed to Li_xSO_y or Li_2S.

Going to the Mage | SEI surface, the XP spectra recorded after sputtering appear rather different compared with those obtained for HOPG. In the F 1s range, the $[TFSI]^-$ anion (F_{TFSI}) is now partly transformed to reduced $[TFSI]^-$ species ($F_{TFSI,red}$; yellow line), which only appeared in very low concentrations on HOPG. Another part is transformed to LiF, which was the dominant product upon sputtering of the HOPG substrate. The increase of the total peak area in both the F 1s and the Li 1s spectra after 5 min, where the former is much more pronounced, indicates that Li-containing species like $LiNSO_2CF_3$, LiC_xH_yN, and Li_xSO_y within the SEI are either exposed or formed upon sputtering. In contrast to the system HOPG | SEI, where LiF was formed as the main product during sputtering, sputtering of the SEI formed on the Mage substrate (for 5 min) results mainly in reduced $[TFSI]^-$ decomposition products, as concluded from the lower F 1s BE of these species. We cannot exclude, however, that longer sputter times may also lead to LiF formation. In the N 1s, O 1s, and S 2p spectral ranges, we did not observe any pronounced changes upon sputtering. The C_{sub} peak in the C 1s range still appears with rather low intensity, which means that the surface is still covered with an at least >6–9 nm thick SEI layer after 5 min of sputtering. This is distinctly different from the HOPG | SEI surface, where the C_{sub} peak strongly increased after 10 min of sputtering. It seems that the SEI layers remaining after DMC rinsing were quite different in thickness on HOPG and on Mage. This fits well with the much higher currents and, most likely, more effective SEI formation during electrochemical cycling of the Mage powder electrode compared with the basal HOPG plane.

Conclusions

Aiming at a better understanding of the formation and composition of the SEI layer on carbon electrodes in an ionic liquid electrolyte ([BMP][TFSI] + 0.1 M LiTFSI), we have investigated

these aspects on two very different carbon electrodes (HOPG and more realistic Mage powder electrodes) by half-cell measurements and subsequent ex situ XPS characterization, including also measurements after partial removal of the SEI by sputtering. Comparing these results with data obtained on films created by i) chemical reaction between [BMP][TFSI] multilayer films and post-deposited Li under UHV conditions on HOPG, ii) long-term exposure of HOPG to a [BMP][TFSI] + 0.1 M LiTFSI electrolyte under open circuit conditions, and iii) electrochemically cycled HOPG and Mage model electrodes in [BMP][TFSI] + 0.1 M LiTFSI, we arrive at the following conclusions:

1) Self-poisoning, reductive $[TFSI]^-$ decomposition takes place on both HOPG and Mage electrodes in the first cycle. The CV recorded on Mage furthermore features several (reversible) peaks in the cathodic cycle, which we assign to co-intercalation and decomposition of $[BMP]^+$. This also leads to surface passivation, inhibiting this process after a few cycles.
2) The addition of Li to multilayers of [BMP][TFSI] on the HOPG substrate in UHV leads mainly to the chemical decomposition of $[BMP]^+$, resulting in products like Li_3N and LiC_xH_yN, whereas electrochemical cycling results predominantly in $[TFSI]^-$ decomposition to, for example, LiF, $LiNSO_2CF_3$, and $-CF_3$ species.
3) $[TFSI]^-$ decomposes mainly to LiF on HOPG. An additional, unidentified F-containing species is observed for the Mage surface, which we assign to reduced $[TFSI]^-$ species.
4) Depth profiling by Ar^+ sputtering may lead to the formation of new decomposition products that are not present in the SEI layer originally. For example, sputtering of LiTFSI produces a large amount of reduced $[TFSI]^-$ decomposition products and LiF after a short time. Similar products are observed also for the electrochemically formed SEI layer, both before and after sputtering. The fact that these products are present already before sputtering indicates that they are formed by electrochemical cycling, whereas after sputtering they can result from either sputter decomposition or electrochemical decomposition.

We believe that this kind of model study is crucial for a detailed, fundamental understanding of battery interfaces and interphases. As such, they constitute the first step towards a systematic further improvement of LIB safety and stability.

Experimental Section

Ultrahigh vacuum (UHV) experiments

All experiments were performed in a commercial UHV system (SPECS) equipped with standard facilities for surface preparation and characterization, which have been described in detail elsewhere.[28] X-ray photoelectron spectroscopy (XPS) measurements were performed with an standard X-ray source (SPECS XR50, AlK_α and MgK_α), which was operated at a power of 250 W ($U = 14$ kV, $I = 17.8$ mA), and a hemispherical analyzer (SPECS, DLSEGD-PhoibosHas3500), typically at a base pressure of 2×10^{-10} mbar. We used either an AlK_α or a MgK_α X-ray source (1486.6 and 1253.6 eV, respectively). The ex situ XPS measurements performed after the electrochemical measurements were recorded with a pass energy of 100 eV at emission angles of 0° with respect to the surface normal (information depth 6–9 nm). Measurements on the UHV-prepared samples were performed at the same pass energies, but at grazing emission (80°, surface sensitive mode, information depth of 1–2 nm). To avoid beam damage during X-ray exposure, we minimized the number of scans for all detail spectra.

Highly oriented pyrolytic graphite (HOPG) was purchased from MaTecK (ZYA, $1\times10\times10$ mm, mosaic spread $0.4\pm0.1°$) and prepared by stripping the uppermost graphene layers using adhesive tape. The freshly cleaved HOPG was fixed on a tantalum sample plate, employing conductive silver paste and heated under nitrogen atmosphere for 30 min at 450 °C. Next, the sample was transferred into the UHV chamber and briefly heated up to approximately 900 K to remove residual contaminations from the surface. [BMP][TFSI] (Merck, ultrapure) was filled into a glass crucible in a Knudsen effusion cell (Ventiotec, OVD-3) mounted inside the UHV chamber. Prior to its use, the IL was carefully degassed in UHV at around 400 K for 24 h to generate pure, water-free IL. To form [BMP][TFSI] adlayers on HOPG, the IL (evaporation temperature 450 K) was deposited on the HOPG at room temperature (r.t.) with a deposition rate of 0.1 ML min^{-1}, with one monolayer (ML) being defined as a layer saturating the surface. Lithium deposition was carried out with a deposition rate of approximately 0.04 MLE min^{-1} (monolayer equivalent per minute) by a Li dispenser (SAES Getters, $U = 1.1$ V/$I = 7.1$ A) mounted approximately 6 cm above the HOPG (at r.t.) sample. As a reference sample for the electrochemical experiments, LiTFSI was mounted on a conductive carbon sticker on top of a tantalum sample holder inside a glovebox and transferred to the UHV chamber under inert conditions.

Electrochemical measurements

HOPG electrodes were cleaved as described above. The binder-free powder electrodes were deposited from a sonicated aqueous solution (25 μL) of Mage graphite powder (Hitachi, 4 mg mL^{-1}) on a polished glassy carbon disk and pre-dried under a nitrogen stream. For the electrochemical measurements, we used a custom-made, open Kel-F half-cell with an electrolyte volume of 0.3 mL. The working electrode is situated under an opening in the bottom of the cell body, allowing the use of both HOPG crystals and glassy carbon disks. To prevent electrolyte leakage, an O-ring (FKM 75, inner diameter 5 mm, cross section 1 mm) was placed between the working electrode and cell body. The cell (including the electrode) was dried for 16 h in the glovebox antechamber at 100 °C and then assembled in a three-electrode setup inside the glovebox ($H_2O \leq 1$ ppm/$O_2 \leq 0.5$ ppm). Li foil (Alfa Aesar, ≥ 99.99%) was used as reference and counter electrodes (all potentials mentioned are referenced versus Li/Li^+ if not stated otherwise).

A 0.1 M solution of lithium bis(trifluoromethylsulfonyl) imide (LiTFSI, 99.9%, Solvionic, 0.5% H_2O) in 1-butyl-1-methylpyrrolidinium bis(trifluoromethylsulfonyl) imide ([BMP][TFSI], 99.9%, Solvionic, ≤ 20 ppm H_2O) was prepared in a glovebox. Electrolyte (0.3 mL) was filled into the completely assembled cell, both for the measurement kept at OCP for 68 h and for the potential cycling experiments.

Cyclic voltammograms were recorded at scan rates of 0.1, 1, and 10 mV s^{-1} in a potential window of 1.5–0.02 V by using a Princeton potentiostat (PAR 263A). The resulting currents were normalized by the geometric surface area of the electrode ($SA_{geo} = 0.196$ cm^2). For X-ray photoelectron spectroscopy (XPS), selected samples were cleaned of excess salt and electrolyte by fourfold solvent exchange using dimethyl carbonate (DMC, 99.9%, Sigma–Aldrich, ≤ 20 ppm H_2O) in the glovebox, followed by a 45–60 min soaking period in

DMC. This cleaning process was repeated five times. After a 45–60 min drying period, the cell was disassembled and the electrode was transferred to the spectrometer in a hermetically sealed transport box excluding contact to air.

XPS data evaluation

The resulting XP spectra were evaluated by using a semi-quantitative approach similar to the one described in detail in ref. [62]. Briefly, all binding energy scales were calibrated by using the F 1s peak of $[TFSI]^-$ at 689.3 eV as reference. We subtracted a Shirley-type background and applied a weighed least-square fit of model curves (70% Gaussian, 30% Lorentzian) for the peak fit. Atomic concentrations were determined by using atomic sensitivity factors (ASF), which were determined from a reference sample (sample a in Figure 3; for the ASFs used see Table S1 in the Supporting Information), consisting of a multilayer film of [BMP][TFSI] on HOPG after deposition of 10 ML of [BMP][TFSI] by correlating the measured intensities to the nominal atomic ratios within the ionic liquid (N_{BMP}/N_{TFSI} 1:1, $C_{TFSI}/C_{hetero}/C_{alkyl}$ 2:4:5, F_{TFSI}/C_{TFSI} 6:2, C_{TFSI}/O_{TFSI} 1:2, and O_{TFSI}/S_{TFSI} 2:1).

Acknowledgements

We gratefully acknowledge financial support by the German Federal Ministry of Education and Research (BMBF) in the project 03X4636C ('Li-EcoSafe—Entwicklung kostengünstiger und sicherer Lithium-Ionen-Batterien'), and by the Deutsche Forschungsgemeinschaft via project ID 422053626 (Cluster of Excellence 'Post-Li Storage') and project BE 1201/22-1 ('Zn-Air Batteries'). This work contributes to the research performed at CELEST (Center for Electrochemical Energy Storage Ulm-Karlsruhe).

Conflict of interest

The authors declare no conflict of interest.

Keywords: carbon · electrochemistry · ionic liquid · solid–electrolyte interphase · surface chemistry

[1] J.-M. Tarascon, M. Armand, *Nature* **2001**, *414*, 359 – 367.
[2] B. Scrosati, J. Garche, *J. Power Sources* **2010**, *195*, 2419 – 2430.
[3] B. Scrosati, *Electrochim. Acta* **2000**, *45*, 2461 – 2466.
[4] P. G. Bruce, B. Scrosati, J.-M. Tarascon, *Angew. Chem. Int. Ed.* **2008**, *47*, 2930 – 2946; *Angew. Chem.* **2008**, *120*, 2972 – 2989.
[5] N. Nitta, F. Wu, J. T. Lee, G. Yushin, *Mater. Today* **2015**, *18*, 252 – 264.
[6] D. Aurbach, Y. Talyosef, B. Markovsky, E. Markevich, E. Zinigrad, L. Asraf, J. S. Gnanaraj, H. J. Kim, *Electrochim. Acta* **2004**, *50*, 247 – 254.
[7] K. Xu, *Chem. Rev.* **2004**, *104*, 4303 – 4417.
[8] J. Kalhoff, G. G. Eshetu, D. Bresser, S. Passerini, *ChemSusChem* **2015**, *8*, 2154 – 2175.
[9] M. Galiński, A. Lewandowski, I. Stepniak, *Electrochim. Acta* **2006**, *51*, 5567 – 5580.
[10] M. Ishikawa, T. Sugimoto, M. Kikuta, E. Ishiko, M. Kono, *J. Power Sources* **2006**, *162*, 658 – 662.
[11] H. Liu, Y. Liu, J. Li, *Phys. Chem. Chem. Phys.* **2010**, *12*, 1685 – 1697.
[12] A. Lewandowski, A. Swiderska-Mocek, *J. Power Sources* **2009**, *194*, 601 – 609.
[13] M. Shamsipur, A. A. M. Beigi, M. Teymouri, S. M. Pourmortazavi, M. Irandoust, *J. Mol. Liq.* **2010**, *157*, 43 – 50.
[14] Q. Li, J. Chen, L. Fan, X. Kong, Y. Lu, *Green Energy Environ.* **2016**, *1*, 18 – 42.
[15] D. R. MacFarlane, P. Meakin, J. Sun, N. Amini, M. Forsyth, *J. Phys. Chem. B* **1999**, *103*, 4164 – 4170.
[16] D. R. MacFarlane, M. Forsyth, P. C. Howlett, J. M. Pringle, J. Sun, G. Annat, W. Neil, E. I. Izgorodina, *Acc. Chem. Res.* **2007**, *40*, 1165 – 1173.
[17] D. R. MacFarlane, K. R. Seddon, *Aust. J. Chem.* **2007**, *60*, 3 – 5.
[18] P. Hapiot, C. Lagrost, *Chem. Rev.* **2008**, *108*, 2238 – 2264.
[19] S. K. Martha, E. Markevich, V. Burgel, G. Salitra, E. Zinigrad, B. Markovsky, H. Sclar, Z. Pramovich, O. Heik, D. Aurbach, I. Exnar, H. Buqa, T. Drezen, G. Semrau, M. Schmidt, D. Kovacheva, N. Saliyski, *J. Power Sources* **2009**, *189*, 288 – 296.
[20] S. Menne, J. Pires, M. Anouti, A. Balducci, *Electrochem. Commun.* **2013**, *31*, 39 – 41.
[21] L. Lombardo, S. Brutti, M. A. Navarra, S. Panero, P. Reale, *J. Power Sources* **2013**, *227*, 8 – 14.
[22] R. A. Di Leo, A. C. Marschilok, K. J. Takeuchi, E. S. Takeuchi, *Electrochim. Acta* **2013**, *109*, 27 – 32.
[23] A. Lahiri, T. J. S. Schubert, B. Iliev, F. Endres, *Phys. Chem. Chem. Phys.* **2015**, *17*, 11161 – 11164.
[24] P. Verma, P. Maire, P. Novák, *Electrochim. Acta* **2010**, *55*, 6332 – 6341.
[25] M. Gauthier, T. J. Carney, A. Grimaud, L. Giordano, N. Pour, H. H. Chang, D. P. Fenning, S. F. Lux, O. Paschos, C. Bauer, M. Filippo, S. Lupart, P. Lamp, Y. Shao-Horn, *J. Phys. Chem. Lett.* **2015**, *6*, 4653 – 4672.
[26] S. J. An, J. Li, C. Daniel, D. Mohanty, S. Nagpure, D. L. Wood III, *Carbon* **2016**, *105*, 52 – 76.
[27] E. Peled, S. Menkin, *J. Electrochem. Soc.* **2017**, *164*, A1703 – A1719.
[28] F. Buchner, B. Uhl, K. Forster-Tonigold, J. Bansmann, A. Groß, R. J. Behm, *J. Chem. Phys.* **2018**, *148*, 193821.
[29] B. Uhl, M. Roos, R. J. Behm, T. Cremer, F. Maier, H. P. Steinrück, *Phys. Chem. Chem. Phys.* **2013**, *15*, 17295 – 17302.
[30] B. Uhl, F. Buchner, S. Gabler, M. Bozorgchenani, R. J. Behm, *Chem. Commun.* **2014**, *50*, 8601 – 8604.
[31] B. Uhl, H. Huang, D. Alwast, F. Buchner, R. J. Behm, *Phys. Chem. Chem. Phys.* **2015**, *17*, 23816 – 23832.
[32] F. Buchner, M. Bozorgchenani, B. Uhl, H. Farkhondeh, J. Bansmann, R. J. Behm, *J. Phys. Chem. C* **2015**, *119*, 16649 – 16659.
[33] B. Uhl, M. Hekmatfar, F. Buchner, R. J. Behm, *Phys. Chem. Chem. Phys.* **2016**, *18*, 6618 – 6636.
[34] F. Buchner, M. Fingerle, J. Kim, T. Späth, R. Hausbrand, R. J. Behm, *Adv. Mater. Interfaces* **2019**, *6*, 1801650.
[35] J. Kim, I. Weber, F. Buchner, J. Schnaidt, R. J. Behm, *J. Chem. Phys.* **2019**, *151*, 134704.
[36] F. Buchner, K. Forster-Tonigold, M. Bozorgchenani, A. Gross, R. J. Behm, *J. Phys. Chem. Lett.* **2016**, *7*, 226 – 233.
[37] F. Buchner, J. Kim, C. Adler, M. Bozorgchenani, J. Bansmann, R. J. Behm, *J. Phys. Chem. Lett.* **2017**, *8*, 5804 – 5809.
[38] P. C. Howlett, D. R. MacFarlane, A. F. Hollenkamp, *Electrochem. Solid-State Lett.* **2004**, *7*, A97 – A101.
[39] P. C. Howlett, N. Brack, A. F. Hollenkamp, M. Forsyth, D. R. MacFarlane, *J. Electrochem. Soc.* **2006**, *153*, A595 – A606.
[40] P. C. Howlett, E. I. Izgorodina, M. Forsyth, D. R. MacFarlane, *Z. Phys. Chem.* **2006**, *220*, 1483 – 1498.
[41] S. Randström, G. B. Appetecchi, C. Lagergren, A. Moreno, S. Passerini, *Electrochim. Acta* **2007**, *53*, 1837 – 1842.
[42] S. Randström, M. Montanino, G. B. Appetecchi, C. Lagergren, A. Moreno, S. Passerini, *Electrochim. Acta* **2008**, *53*, 6397 – 6401.
[43] Y. Shi, H. J. Yan, R. Wen, L. J. Wan, *ACS Appl. Mater. Interfaces* **2017**, *9*, 22063 – 22067.
[44] V. Baranchugov, E. Markevich, G. Salitra, D. Aurbach, G. Semrau, M. A. Schmidt, *J. Electrochem. Soc.* **2008**, *155*, A217 – A227.
[45] A. M. O'Mahony, D. S. Silvester, L. Aldous, C. Hardacre, R. G. Compton, *J. Chem. Eng. Data* **2008**, *53*, 2884 – 2891.
[46] N. De Vos, C. Maton, C. V. Stevens, *ChemElectroChem* **2014**, *1*, 1258 – 1270.
[47] D. Alwast, J. Schnaidt, K. Hancock, G. Yetis, R. J. Behm, *ChemElectroChem* **2019**, *6*, 3009 – 3019.
[48] M. Tułodziecki, J.-M. Tarascon, P. L. Taberna, C. Guéry, *Electrochem. Commun.* **2017**, *77*, 128 – 132.
[49] X. Hu, C. Chen, J. Yan, B. Mao, *J. Power Sources* **2015**, *293*, 187 – 195.
[50] G. B. Appetecchi, M. Montanino, A. Balducci, S. F. Lux, M. Winter, S. Passerini, *J. Power Sources* **2009**, *192*, 599 – 605.

[51] S. K. Jeong, M. Inaba, Y. Iriyama, T. Abe, Z. Ogumi, *Electrochim. Acta* **2002**, *47*, 1975 – 1982.
[52] C. Shen, S. Wang, Y. Jin, W. Q. Han, *ACS Appl. Mater. Interfaces* **2015**, *7*, 25441 – 25447.
[53] L. H. S. Gasparotto, N. Borisenko, N. Bocchi, S. Z. El Abedin, F. Endres, *Phys. Chem. Chem. Phys.* **2009**, *11*, 11140 – 11145.
[54] E. Markevich, V. Baranchugov, G. Salitra, D. Aurbach, M. A. Schmidt, *J. Electrochem. Soc.* **2008**, *155*, A132 – A137.
[55] E. Markevich, R. Sharabi, V. Borgel, H. Gottlieb, G. Salitra, D. Aurbach, G. Semrau, M. A. Schmidt, *Electrochim. Acta* **2010**, *55*, 2687 – 2696.
[56] M. Nádherná, J. Reiter, J. Moskon, R. Dominko, *J. Power Sources* **2011**, *196*, 7700 – 7706.
[57] G. B. Appetecchi, M. Montanino, D. Zane, M. Carewska, F. Alessandrini, S. Passerini, *Electrochim. Acta* **2009**, *54*, 1325 – 1332.
[58] M. Winter, J. O. Besenhard, M. E. Spahr, P. Novák, *Adv. Mater.* **1998**, *10*, 725 – 763.
[59] B. Jungblut, E. Hoinkis, *Phys. Rev. B* **1989**, *40*, 10810.
[60] T. Tran, K. Kinoshita, *J. Electroanal. Chem.* **1995**, *386*, 221 – 224.
[61] F. Buchner, K. Forster-Tonigold, J. Kim, C. Adler, J. Bansmann, A. Groß, R. J. Behm, *J. Phys. Chem. C* **2018**, *122*, 18968 – 18981.
[62] I. Weber, J. Schnaidt, B. Wang, T. Diemant, R. J. Behm, *ChemElectroChem* **2019**, *6*, 4985 – 4997.
[63] H. Zheng, K. Jiang, T. Abe, Z. Ogumi, *Carbon* **2006**, *44*, 203 – 210.
[64] J. F. Moulder, W. F. Stickle, P. E. Sobol, K. D. Bomben, *Handbook of X-ray Photoelectron Spectroscopy*, PerkinElmer Corp., Eden Prairie, USA, **1992**.
[65] T. Cremer, M. Stark, A. Deyko, H. P. Steinrück, F. Maier, *Langmuir* **2011**, *27*, 3662 – 3671.
[66] Y. Ando, Y. Kawamura, T. Ikeshoji, M. Otani, *Chem. Phys. Lett.* **2014**, *612*, 240 – 244.
[67] D. Aurbach, A. Zaban, Y. Ein-Eli, I. Weissman, O. Chusid, B. Markovsky, M. Levi, E. Levi, A. Schechter, E. Granot, *J. Power Sources* **1997**, *68*, 91 – 98.
[68] C. Xu, B. Sun, T. Gustafsson, K. Edström, D. Brandell, M. Hahlin, *J. Mater. Chem. A* **2014**, *2*, 7256 – 7264.
[69] K. Park, B. C. Yu, J. B. Goodenough, *Adv. Energy Mater.* **2016**, *6*, 1502534.
[70] M. Olschewski, R. Gustus, M. Marschewski, O. Höfft, F. Endres, *Phys. Chem. Chem. Phys.* **2014**, *16*, 25969 – 25977.
[71] D. R. MacFarlane, J. M. Pringle, P. C. Howlett, M. Forsyth, *Phys. Chem. Chem. Phys.* **2010**, *12*, 1659 – 1669.
[72] M. Yamagata, N. Nishigaki, S. Nishishita, Y. Matsui, T. Sugimoto, M. Kikuta, T. Higashizaki, M. Kono, M. Ishikawa, *Electrochim. Acta* **2013**, *110*, 181 – 190.
[73] A. Lahiri, T. Carstens, R. Atkin, N. Borisenko, F. Endres, *J. Phys. Chem. C* **2015**, *119*, 16734 – 16742.
[74] G. Giffin, A. Moretti, S. Jeong, S. Passerini, *J. Phys. Chem. C* **2014**, *118*, 9966 – 9973.

Manuscript received: February 24, 2020
Accepted manuscript online: March 20, 2020
Version of record online: April 24, 2020